Boosting Road Damage Detection via DEMATEL with Bipolar Neutrsophic Dombi for Intelligent Smart City Infrastructure

Imène Issaoui[1,*], Afef Selmi[2]

[1]Unit of Scientific Research, Applied College, Qassim University, Buraydah, Saudi Arabia

[2]Department of Information Technology, College of Computer, Qassim University, Buraydah, Saudi Arabia

Emails: i.issaoui@qu.edu.sa; a.selmi@qu.edu.sa

Abstract

In decision-making, NS permits the representation of information with three membership functions: indeterminacy (I), false (F), and truth (T). All components in an NS have indeterminacy, non-, and membership degrees that are autonomous and vary from (0-1). This generates NS particularly appropriate in composite decision-making situations where information is incomplete, ambiguous, or contradictory, which allows strong and more complex solutions and analysis. Detecting road damage accurately and quickly enables the capability of road maintenance agencies to generate timely maintenance to road surfaces, retain optimum road conditions, enhance the safety of transportation, and reduce transportation charges. Research on road damage detection using AI models achieved more attention at present, particularly in smart cities. This paper develops a Boosting Road Damage Detection using DEMATEL with Bipolar Neutrosophic Dombi and Siberian Tiger Optimization (BRDD-DBNDSTO) algorithm. The presented BRDD-DBNDSTO technique is mainly intended to improve the accuracy and reliability of road damage classification for intelligent smart city infrastructure. To accomplish this, the BRDD-DBNDSTO technique employs adaptive bilateral filtering (ABF) using image preprocessing to effectively enhance image quality by reducing noise. Then, the SqueezeNet method was used to create a collection of feature vectors. For the classification and detection of road damage, the DEMATEL with bipolar neutrosophic Dombi model is exploited. At last, the Siberian tiger optimization (STO) algorithm is used to adjust the parameters related to the classifier model. To guarantee the improved performance of the BRDD-DBNDSTO method, an extensive experimental study was carried out and the gained outcomes illustrate the improvement of the BRDD-DBNDSTO model across the existing techniques.

Keywords: Bipolar Neutrosophic Set; DEMATEL; Bipolar Neutrosophic Dombi; Road Damage Detection; Siberian Tiger Optimization

1. Introduction

To deal with inconsistency and uncertainty is a major importance problem for investigators that research mathematical representation [1]. Investigators have presented several estimates to make mathematical modeling some difficulties comprising inconsistency and uncertainty data. A few famous estimates are fuzzy set concept presented and intuitionistic fuzzy set (IFS) concept presented. A fuzzy set (FS) was recognized by membership function and an IFS was recognized by non- and membership functions [2]. Nevertheless, FSs and IFSs do not process the inconsistent and indeterminant information. Hence, neutrosophic set (NS) concept was presented as a generality of FS and IFS depending on Neutrosophy which is a subdivision of philosophy. Roadways are significant public properties that offer noticeable, longer-range advantages to society because they encourage financial growth in markets by guaranteeing mobility and admittance for people and goods [3]. Preserving roads immediately in perfect condition is crucial to the keenness and maintainable growth of national, regional, and local markets [4]. Road infrastructure should be properly retained to withstand and exploit these advantages which need road maintenance specialists to have required support and strong devices to precisely respond to road condition

DOI: https://doi.org/10.54216/IJNS.250318
Received: June 06, 2024 Revised: August 27, 2024 Accepted: October 04, 2024

complications [5]. Weak road conditions are the reason for numerous issues such as making road navigation difficulties and raising accident risk for drivers, growing repair costs for vehicles by using these roads, and eventually high road-repair costs owing to irreversible decline of road substructures and surfaces [6].

Furthermore, it allows the growth of machine learning (ML) methods for automatic detection of road damage, an important device for infrastructure monitoring and disaster awareness. Of the increasing tendency of Artificial Intelligence (AI)-based automating applications, numerous Road Damage Datasets have been presented in the past few years [7]. This has intensely transformed with the initiation of the computer vision (CV) models depending on deep learning (DL) structures, which have established great steps in many CV tasks and have gradually completed their method into road inspection methods [8]. The usage of DL can play an important part in resolving real-world difficulties after the developments in computer schemes, mainly graphical processing units (GPUs) [9]. The Automation of DL in domains of different fields can be simple, like agriculture, proper water resources supply, medical, in-city surveillance, and facial expression identification. Recently, the most stimulating subject was cracks, damage, and pothole recognition of road surfaces using AI [10]. Particularly, DL offers numerous study models to recognize loss to road surfaces.

This paper develops a Boosting Road Damage Detection using DEMATEL with Bipolar Neutrosophic Dombi and Siberian Tiger Optimization (BRDD-DBNDSTO) algorithm. To accomplish this, the BRDD-DBNDSTO technique employs adaptive bilateral filtering (ABF) using image preprocessing to effectively enhance image quality by reducing noise. Then, the SqueezeNet method was used to create a collection of feature vectors. For the classification and detection of road damage, the DEMATEL with bipolar neutrosophic Dombi model is exploited. At last, the Siberian tiger optimization (STO) algorithm is used to adjust the parameters related to the classifier model. To guarantee the improved performance of the BRDD-DBNDSTO model, an comprehensive empirical study was conducted, and the results showed that the BRDD-DBNDSTO technique outperforms recent methods.

2. Related Works

Merolla et al. [11] proposed a new model for enhancing road security over the classification and detection of traffic signs and road surface damage with progressive DL algorithms. This combined model supports dynamic maintenance approaches, enhancing road security and allocation of resources for the Molise area and the Campobasso city. The resultant method uses cutting-edge technology like Cloud Computing and Higher-Performance Computing with GPU application. Chu et al. [12] presented a decision support system (DSS) for an independent road information scheme for smart cities improvement by the usage of DL. The introduced DSS mechanisms in layers while primarily the road images were coordinates and captured assigned to the image using the GPS assistance, interconnected to the decision layer to discover the potholes and cracks, which provided data to the maintenance department and the drivers. CNN-based method has been presented for pothole crack detection (PCD), for the decision layer. Adewopo and Elsayed [13] implemented a complete exploration learning of main accidental detection methods, flaking light on the degrees of further advanced methods while giving a complete summary of different traffic accidental kinds such as T-bone collisions, rear-end collisions, and frontal influence accidents. This new model presented the I3D-CONVLSTM2D architectural method, a lightweight solution tailor-made clearly for accidental detection in smart cities traffic monitoring.

Silva et al. [14] introduced an original automatic road damage detection model using UAV images and DL algorithms. Conserving road structure is crucial to ensure a safer and supportable transportation system. Nevertheless, the physical set of road loss data is unsafe and time-consuming for humans. Hence, UAVs and AI technology are presented to increase road damage detection's accuracy and efficiency considerably. In [15], a complete vehicle security structure tailor-made especially for smart cities in AIoT has been presented. This structure combines a particular sensor that successfully monitors the alcohol content of drivers. In cases of higher alcohol levels, the method uses GSM and GPS technologies to spontaneously regulate the speed of vehicles while instantaneously informing relevant experts for quick intervention. In [16], a solution of RHD depending on CVIS was presented. Initially, a higher-execution heavy action detection method was designated. With a meta-learning model, crucial features are simplified from fewer-shot data of RH. Then, a lightweight RHD method was calculated to guarantee its smoother implication on an OCD. Finally, a knowledge distillation (KD) architecture has been applied to increasingly distillation the features.

3. Materials and Methods

In this article, we have presented a new BRDD-DBNDSTO algorithm. The proposed BRDD-DBNDSTO approach is mainly intended to enhance the accuracy and reliability of road damage classification for intelligent smart city infrastructure. To accomplish this, the BRDD-DBNDSTO technique has classification, feature extraction, image pre-processing, and hyperparameter tuning are depicted in Fig. 1.

DOI: https://doi.org/10.54216/IJNS.250318
Received: June 06, 2024 Revised: August 27, 2024 Accepted: October 04, 2024

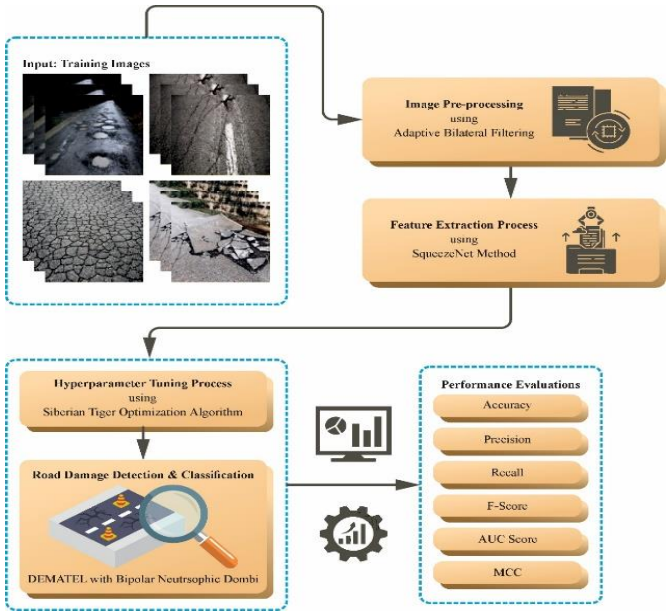

Figure 1. Overall flow of BRDD-DBNDSTO algorithm

A. Image Preprocessing: ABF Model

Primarily, the BRDD-DBNDSTO technique employs ABF using image preprocessing to effectively enhance image quality by reducing noise. ABF is a critical image preprocessing model in the detection of road damage, as it efficiently decreases noise while maintaining significant important details in road surface images [17]. This method improves the visibilities of refined damage features, allowing more precise classification and feature extraction. By increasing image qualities, ABF makes a major contribution to the strength of ML methods employed in automatic road condition estimations.

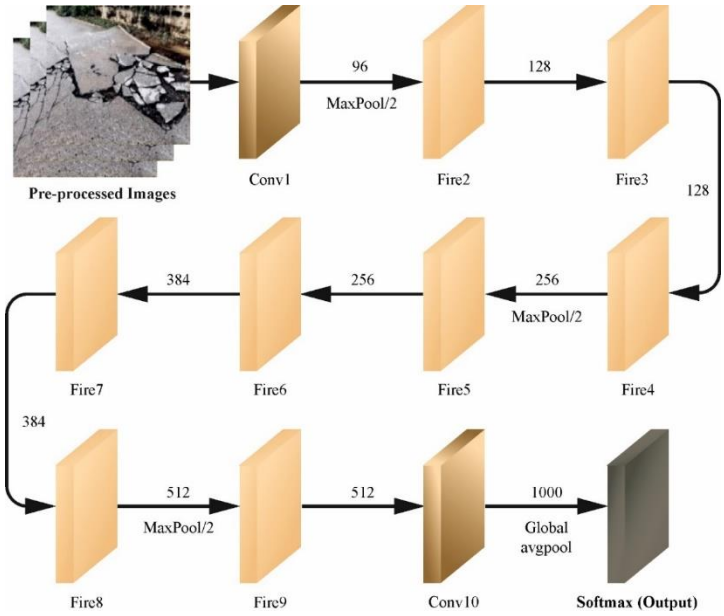

Figure 2. Structure of SqueezeNet

B. Feature Extraction: SqueezeNet

Then, the SqueezeNet method was used to create a collection of feature vectors. SqueezeNet is chosen for the developed research [18]. The structure of CNN was presented in the year 2016. It is recognized for its effective design, which has very little computational complexity necessities. However, it upholds great accuracy even with these complex needs. It contains 8 fire blocks (fire2 to fire9), a convolutional layer (Conv1), and a last convolutional layer (Conv10). The Fire block is the main advance in SqueezeNet. It is a specific module that is

DOI: https://doi.org/10.54216/IJNS.250318
Received: June 06, 2024 Revised: August 27, 2024 Accepted: October 04, 2024

intended to improve the efficiency of the network. Every fire block starts with a layer of squeeze. It includes a set of 1x1 convolutional filters. This squeeze layer decreases the intensity of input data by compacting its features. Therefore, it limits the amount of input channels to the following layers. After the squeeze layer, the structure divides into dual layers of expansion, one with 3x3 convolutional filters and the other with 1x1 convolutional filters. This mixture of squeeze-and-expand mechanism lets SqueezeNet decrease the size of the model and computational needs. Fig. 2 represents the framework of SqueezeNet.

C. Classification: DEMATEL with Bipolar Neutrosophic Dombi

For the classification and detection of road damage, the DEMATEL with bipolar neutrosophic Dombi model is exploited. The below-mentioned section provides a summary of the descriptions linked to the Heronian mean (HM), bipolar neutrosophic set (BNS), and Bipolar Neutrosophic Dombi-based Improved Generalized Weighted Heronian mean (BND-IGWHM) operators [19]. These definitions are mainly employed in incorporating the BND-IGWHM operator into the DEMATEL model.

Definition1. BNS

Assume X as a set of non-empty. A BNS A is described as demonstrated:

$$A = \{\{x, T^+(x), I^+(x), F^+(x), T^-(x), I^-(x), F^-(x)\} : x \in X\}, \quad (1)$$

where $T^+, I^+, F^+ : X \to [1,0]$ and $T^-, I^-, F^- : X \to [-1,0]$.

Here, the $T^+(x), I^+(x), F^+(x)$ signifies positive membership degree, whereas $T^-(x), I^-(x), F^-(x)$ is negative membership degree of an element $x \in X$.

Definition2. Deneutrosophication of BNS

Assume that $4_j = \langle t_{ij}^+, i_{ij}^+, f_{ij}^+, t_{i_j}^-, i_{i_j}^-, f_{i_j}^- \}$ is a BNS. Deneutrosophication of A_{ij} is well-defined as below:

$$\mu(A_{ij}) = 1 - \left[\frac{1}{2}\sqrt{\left(\frac{(1-t_{ij}^+)^2 + (i_{ij}^+)^2 + (f_{ij}^+)^2}{3}\right) + \left(\frac{(1-(-t_{ij}^-))^2 + (-i_{ij}^-)^2 + (-f_{ij}^-)^2}{3}\right)}\right] \quad (2)$$

Definition3. BND- IGWHM

Let $p, q \geq 0, \gamma > 0$, and $A_{ij}^K = \langle t_{\text{ij}}^{+K}, i_{\text{ij}}^{+K}, f_{ij}^{+K}, t_{ij}^{-K}, i_{ij}^{-K}, f_{\text{ij}}^{-K} \rangle$ is a relation of BNS with weight $w_k = (w_1, w_2, \dots, w_m)^T$ fulfilling $w_k \in [0,1]$ and $\sum_{r=1}^m w_k = 1$. Next, $BND - IGWHM^{p,q}$ is named (BND-IGWHM) operator and is specified by

$$BND - IGWHM^{p,q}(A_{ij}^1, A_{ij}^2, \dots, A_{ij}^m) = \frac{\left(\sum_{k=1}^m \sum_{s=k}^m w_k\, w_s A_{ij}^{kp} \otimes A_{ij}^{sq}\right)^{\frac{1}{p+q}}}{\left(\sum_{k=1}^m \sum_{s=k}^m w_k\, w_s\right)^{\frac{1}{p+q}}}$$

$$=< \left(1 + \left(\left(\frac{\sum_{k=1}^m \sum_{s=k}^m w_k\, w_s}{p+q}\right) \times 1/\left(\sum_{k=1}^m \sum_{k=r}^m (w_k w_s / \left(p\left(\frac{1-t_{ij}^{+k}}{t_{ij}^{+k}}\right)^\gamma\right)\left(q\left(\frac{1-t_{ij}^{+s}}{t_{ij}^{+s}}\right)^\gamma\right)\right)^{\frac{1}{\gamma}}\right)\right)^{-1}$$

$$1 - \left(1 + \left(\left(\frac{\sum_{r=1}^m \sum_{s=r}^m w_i\, w_j}{p+q}\right) \times 1/\left(\sum_{r=1}^m \sum_{s=r}^m w_r\, w_s / \left(\left(p\left(\frac{i_{ij}^{+r}}{1-i_{ij}^{+r}}\right)^\gamma\right) + \left(q\left(\frac{i_{ij}^{+s}}{1-i_{ij}^{+s}}\right)^\gamma\right)\right)\right)^{\frac{1}{\gamma}}\right)^{-1}$$

DOI: https://doi.org/10.54216/IJNS.250318
Received: June 06, 2024 Revised: August 27, 2024 Accepted: October 04, 2024

$$1-\left(1+\left(\left(\frac{\sum_{k=1}^{m}\sum_{s=k}^{m}w_k w_s}{p+q}\right)\times 1/\left(\sum_{k=1}^{m}\sum_{s=k}^{m}\left(w_k w_s/\left(\left(p\left(\frac{f_{ij}^{+k}}{1-f_{ij}^{+k}}\right)^{\gamma}\right)+\left(q\left(\frac{f_{ij}^{+s}}{1-f_{ij}^{+s}}\right)^{r}\right)\right)\right)\right)^{\frac{1}{\gamma}}\right)^{-1}, (3)$$

$$\left(1+\left(\left(\frac{\sum_{k=1}^{m}\sum_{s=k}^{m}w_k\, w_s}{p+q}\right)\times 1/\left(\sum_{k=1}^{m}\sum_{s=k}^{m}\left(w_k w_s/\left(\left(p\left(\frac{-t_{ij}^{-k}}{1+t_{ij}^{-k}}\right)^{\gamma}\right)+\left(q\left(\frac{-t_{ij}^{-s}}{1+t_{ij}^{-s}}\right)^{\gamma}\right)\right)\right)\right)^{\frac{1}{\gamma}}\right)^{-1}-1,$$

$$-\left(1+\left(\left(\frac{\sum_{k=1}^{m}\sum_{s=k}^{m}w_k\, w_s}{p+q}\right)\times 1/\left(\sum_{k=1}^{m}\sum_{s=k}^{m}\left(w_k w_s/\left(\left(p\left(\frac{1+i_{ij}^{-k}}{-i_{ij}^{-k}}\right)^{\gamma}\right)+\left(q\left(\frac{1+i_{j}^{-s}}{-i_{j}^{-s}}\right)^{\gamma}\right)\right)\right)\right)^{\frac{1}{\gamma}}\right)^{-1}<$$

$$-\left(1+\left(\left(\frac{\sum_{k=1}^{m}\sum_{s=k}^{m}w_k\, w_s}{p+q}\right)\times 1\left(\sum_{k=1}^{m}\sum_{s=k}^{m}\left(w_k w_s\left(\left(p\left(\frac{1+f_{ij}^{-k}}{-f_{ij}^{-k}}\right)^{\gamma}\right)+\left(q\left(\frac{1+f_{ij}^{-s}}{-f_{ij}^{-s}}\right)^{\gamma}\right)\right)\right)\right)^{\frac{1}{\gamma}}\right)^{-1}$$

This section suggests a variation of DEMATEL called BND-IGWHM DEMATEL, which is mainly beneficial for resolving clusters of decision-making. Let that there are n measures of the problem definite as $C=\{C_1, C_2, \dots, C_n\}$. Assume that $K=\{K_1, K_2, \dots, K_m\}$ is set of experts and $w_r=\{r=1,2, \dots, m\}$ denotes the corresponding weight of experts whereas $0 \le w_r \le 1$ and $\sum_{r=1}^{m} w_r = 1$. The conditions were assessed by specialists utilizing the Bipolar neutrosophic linguistic variable.

Algorithm

Step 1: Build the direct-relation matrices.

Assume $X^K=(A_{ij}^K)_{n\times n}$ as the direct-relation matrices, which are defined as

$$X^K=(A_{ij}^K)_{n\times n}=\begin{bmatrix}0 & A_{12}^K & \dots & A_{1n}^K\\ A_{21}^K & 0 & \dots & A_{2n}^K\\ \vdots & \vdots & \ddots & \vdots\\ A_{n1}^K & A_{n2}^K & \dots & 0\end{bmatrix}, \quad (4)$$

Here, A_{ij} Denotes the Bipolar neutrosophic linguistic variables signifying the grade of influence amongst the criteria of i and j, set by the Kth expert. The option of Bipolar neutrosophic variable, which ranges from "no influence (NI)" to "very high influence (VHI)".

Step 2: Accumulate the direct-relation matrices.

The direct-relation matrices in BNSs are combined utilizing the BND-IGWHM operator, which is definite by Eq. (3). The aggregated direct-relation matrix is signified as A, so

$$A=(A_{ij})_{n\times n}=\begin{bmatrix}0 & A_{12} & \dots & A_{1n}\\ A_{21} & 0 & \dots & A_{2n}\\ \vdots & \vdots & \ddots & \vdots\\ A_{n1} & A_{n2} & \dots & 0\end{bmatrix} \quad (5)$$

where $A_{ij}=BND-IGWHM^{p,q}\left(A_{ij}^1, A_{ij}^2, \dots, A_{ij}^m\right)$

$$=\left\{t_{ij}^{+}, i_{ij}^{+}, f_{\mathrm{ij}}^{+}, t_{\mathrm{ij}}^{-}, i_{\mathrm{ij}}^{-}, f_{\mathrm{ij}}^{-}\right\}, i, j=1,2, \dots, n.$$

Step 3: Calculate the deneutrosophication of Bipolar neutrosophic.

DOI: https://doi.org/10.54216/IJNS.250318
Received: June 06, 2024 Revised: August 27, 2024 Accepted: October 04, 2024

Deneutrosophication is the procedure of attaining crisp numbers from Bipolar neutrosophic numbers. From the aggregated matrix, A is computed utilizing Eq. (2). Assume 4_J as a crisp number matrix, then the crisp matrix, A' is signified as below:

$$A' = (A'_{ij})_{n\times n} = \begin{bmatrix} 0 & A'_{12} & \dots & A'_{1n} \\ A'_{21} & 0 & \dots & A_{2n} \\ \vdots & \vdots & \ddots & \vdots \\ A'_{n1} & A_{n2} & \dots & 0 \end{bmatrix} \tag{6}$$

Step 4: Normalize the section from direct-relation matrix D, which is originated utilizing Eq. (7).

$$D = \frac{1}{s}A', \tag{7}$$

whereas

$$s = \max\left(\max_{1\le i\le n}\sum_{j=1}^{n} A'_{ij}, \max_{1\le j\le n}\sum_{i=1}^{n} A'_{ij}\right) \tag{8}$$

and the matrix D is stated below:

$$D = (A^{"}_{ij})_{n\times n} = \begin{bmatrix} 0 & A^{"}_{12} & \dots & A^{"}_{1n} \\ A^{"}_{21} & 0 & \dots & A^{"}_{2n} \\ \vdots & \vdots & \ddots & \vdots \\ A^{"}_{n1} & A^{"}_{n2} & \dots & 0 \end{bmatrix} \tag{9}$$

From Eq. (7) and (8), the element of $A^{"}_{ij} = \frac{A^{"}_{ij}}{\max_{1\le i\le n}\Sigma_{j=1}^{n} A'_{ij}, \max_{1\le j\le n}\Sigma_{i=1}^{n} A'_{ij}}$, where $0 \le A^{"}_{ij} < 1$.

Step 5: Build the total-relation matrix.

The matrix of total-relation, T is attained by employing Eq. (9), whereas I represents an identity matrix, so

$$T = D(I - D)^{-1} \tag{10}$$

Step 6: Create the causal diagram.

The sum of ith rows (R_i) and jth columns (C_j) of the matrix of total-relation T, are calculated utilizing Eqs. (10) and (11), correspondingly. The horizontal axis $(R_i + C_j)$, called Prominence, displays the ranking of every criterion, while the vertical axis $(R_i - C_j)$, named Relation, measures the cause-effect of the set. If the value of $(R_i - C_j)$ is positive, then the statements state that a factor fits the causal set, and if the value of $(R_i - C_j)$ is negative, then it is an effect group.

$$\eta = [R_i]_{n\times 1} = \sum_{j=1}^{n} [A'''_{ij}]_{n\times 1} (i = 1,2,\dots,n) \tag{11}$$

$$C_j = [C_j]_{1\times n} = \sum_{i=1}^{n} [4'''_j]_{1\times n} (j = 1,2,\dots,n). \tag{12}$$

Step 7: Build the value of threshold and the network relationship map (NRM).

To describe the important relation amongst norms while holding the intricacy of the complete method at a managing level, it's essential to fix a value of threshold t, which performs as a filter on insignificant effected in the matrix of total-relation. The t is described by taking an average of the element in the matrix T. In the matrix T, the elements are expected to be 0 if their values are lesser than t, which indicates that their influence is lesser than those of the other measures. Hence, a novel total-relation matrix can be attained, and a system relationship mapping can be built.

DOI: https://doi.org/10.54216/IJNS.250318
Received: June 06, 2024 Revised: August 27, 2024 Accepted: October 04, 2024

D. Parameter Optimizer: STO Algorithm

Finally, the STO method was used to adjust the parameters associated with the classifier method. At first, start by allocating a randomly generated number to signify the Northeast tiger population [20]. Moreover, randomly define the specific tiger's positions in a pre-defined range. In the hunting stage, the individuals with better values of objective function conclude the recommended prey locations for another individual.

$$PP_j = \{X_k | k \in \{1,2,\dots,N\} \wedge F_k < F_j\} \cup \{X_{best}\} \tag{13}$$

Here, N indicates the numerical value. Pick an individual randomly from this group to be the objective for ith individual's searches.

$$x_{i,j}^{P1S1} = x_{i,j} + r_{i,j} \cdot \left(TP_{i,j} - I_{i,j} \cdot x_{i,j}\right) \tag{14}$$

Whereas, x_i^{P1S1} signifies the revised position of ith individual, $x_{i,j}^{P1S1}$ denotes the jth dimension. When updating individual locations, novel places will help to improve the value of objective function.

$$X_j = \begin{cases} X_i^{P1S1}, & F_i^{P1S1} < F_i \\ X_i, & else \end{cases} \tag{15}$$

While an objective function value signifies the value linked with ith individual.

In second step, individual positions are upgraded as per the hunting method:

$$x_{i,j}^{P1S2} = x_{i,j} + \frac{r_{i,j} \cdot \left(ub_j - lb_j\right)}{t} \tag{16}$$

$$X_i = \begin{cases} X_i^{P1S1}, F_i^{P1S2} < F_i \\ X_i, \quad else \end{cases} \tag{17}$$

Here, X_i^{P1S2} means the revised position of ith individual, F_i^{P1S2} signifies the objective function values.

The phase of battling bears is classified into dual stages such as offensive and confrontational. The spatial position of ith individual is given below:

$$X_{i,j}^{P2S1} = \begin{cases} x_{i,j} + r_{i,j}.\left(x_{k,j} - I_{i,j}.x_{i,j}\right), & F_k < F_l \\ x_{i,j} + r_{i,j}.\left(x_{k,j} - I_{i,j}.x_{i,j}\right), & else \end{cases} \tag{18}$$

Here, X_i^{P2S1} denotes a revised position of ith individual, $X_{i,j}^{P2S1}$ signifies its jth dimension. If an individual's fresh location enhances an amount of the objective function, this new location is studied:

$$X_i = \begin{cases} X_i^{P2S1}, F_i^{P2S1} < F_i \\ X_i, \quad else \end{cases} \tag{19}$$

In the combat stage, the neighboring places to the battle locations are defined at random.

$$x_{i,j}^{P2S2} = x_{i,j} + \frac{r_{i,j}}{t}\left(ub_j - lb_j\right) \tag{20}$$

Here, j ranges from 1 to m; t envelops a range 1 to T; and I ranges from 1 to N.

Alter the present location depending on the objective function values:

$$X_i = \begin{cases} X_i^{P2S2}, & F_i^{P2S2} < F_i \\ X_i, & else \end{cases} \tag{21}$$

The STO method obtains a fitness function (FF) to achieve increased classifier performance. It outlines a positive integer to illustrate the bigger performance of the solutions of the candidate. In this paper, the decline of the classifier rate of error has been determined as the FF.

$$fitness(x_i) = ClassifierErrorRate(x_i)$$

$$= \frac{no\ of\ misclassified\ samples}{Total\ no\ of\ samples} * 100 \tag{22}$$

DOI: https://doi.org/10.54216/IJNS.250318
Received: June 06, 2024 Revised: August 27, 2024 Accepted: October 04, 2024

4. Performance Validation

During this part, the empirical validation of the BRDD-DBNDSTO model has been validated within the dataset. The dataset holds 4000 images over four classes as denoted in Table 1.

Table 1: Details of Dataset

Classes	No. of Images
Linear Cracks	1000
Peeling	1000
Alligator Cracks	1000
Potholes	1000
Total Images	4000

Fig. 3 shows the classifier results of the BRDD-DBNDSTO algorithm. Figs. 3a-3b demonstrate confusion matrix with precise identification and classification of all classes above 70%TRAPH and 30%TESPH. Fig. 3c presents the PR analysis, signifying maximal performance around all class labels. Simultaneously, Fig. 3d represents the ROC investigation, revealing proficient results with high ROC values for discrete class labels.

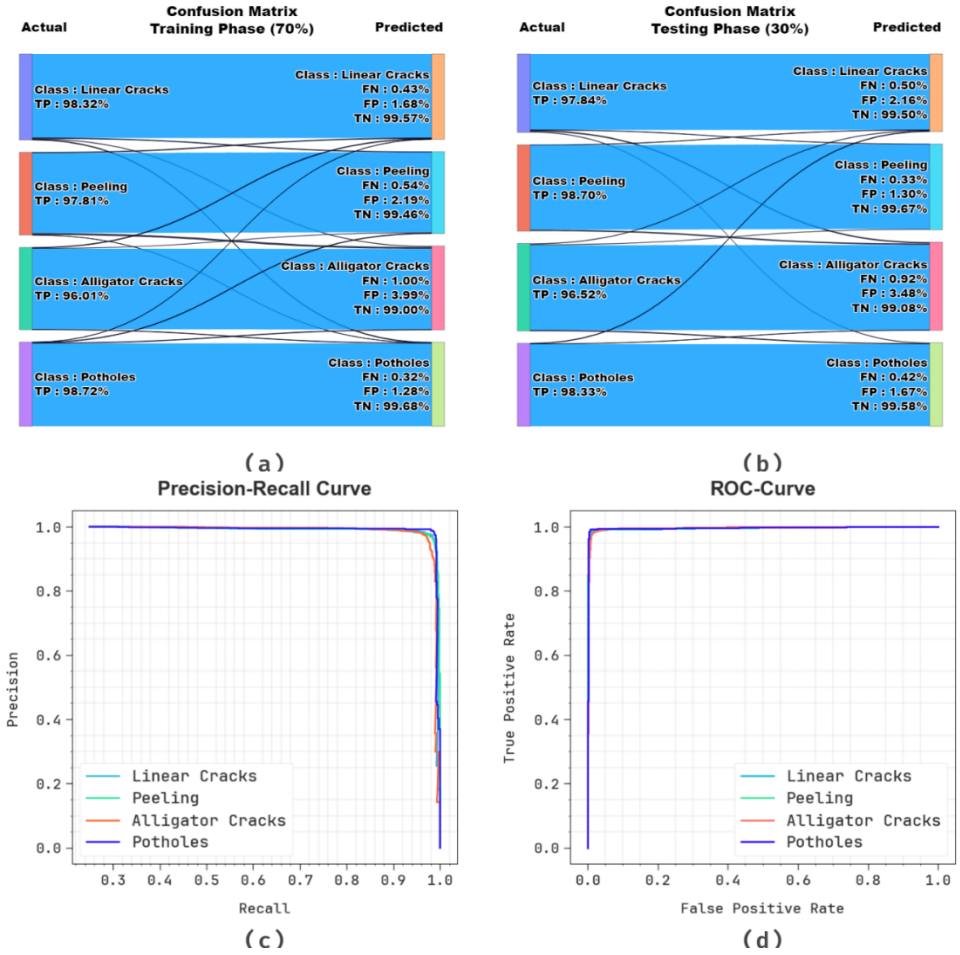

Figure 3. Classifier outcomes of (a-b) 70%TRAPH and 30%TESPH of confusion matrices, (c) curve of PR and (d) curve of ROC

Table 2 and Fig. 4 exemplify the classifier results of the BRDD-DBNDSTO system under 70% TRAPH and 30% TESPH. The results indicate that the BRDD-DBNDSTO algorithm appropriately well-known the samples. With 70%TRAPH, the BRDD-DBNDSTO methodology deals with average $accu_y$, $prec_n$, $reca_l$, $F1_{score}$, AUC_{score} and MCC of 98.86%, 97.71%, 97.71%, 97.71%, 98.48%, and 96.95%, respectively. In the meantime, with 30%TESPH, the BRDD-DBNDSTO model states average $accu_y$, $prec_n$, $reca_l$, $F1_{score}$, AUC_{score} and MCC of 98.92%, 97.85%, 97.82%, 97.83%, 98.55%, and 97.11%, correspondingly.

DOI: https://doi.org/10.54216/IJNS.250318
Received: June 06, 2024 Revised: August 27, 2024 Accepted: October 04, 2024

Table 2: Classifier outcomes of BRDD-DBNDSTO method under 70%TRAPH and 30%TESPH

Classes	$Accu_y$	$Prec_n$	$Reca_l$	$F1_{score}$	AUC_{score}	MCC
70% TRAPH						
Linear Cracks	98.96	98.32	97.64	97.98	98.53	97.28
Peeling	98.68	97.81	96.82	97.31	98.05	96.44
Alligator Cracks	98.50	96.01	97.96	96.97	98.32	95.99
Potholes	99.29	98.72	98.44	98.58	99.00	98.10
Average	98.86	97.71	97.71	97.71	98.48	96.95
30% TESPH						
Linear Cracks	98.75	97.84	96.80	97.32	98.07	96.50
Peeling	99.17	98.70	98.06	98.38	98.80	97.82
Alligator Cracks	98.42	96.52	97.44	96.98	98.10	95.91
Potholes	99.33	98.33	98.99	98.66	99.22	98.22
Average	98.92	97.85	97.82	97.83	98.55	97.11

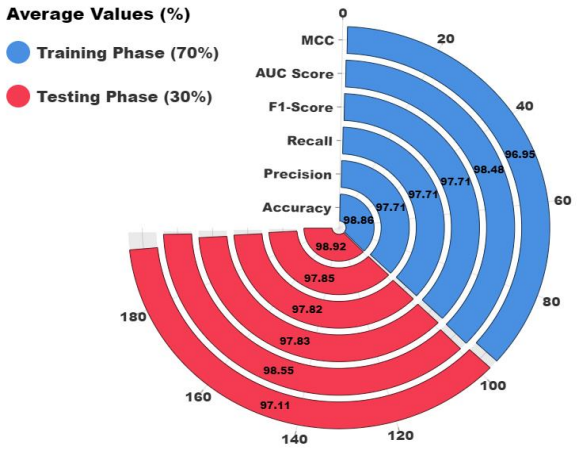

Figure 4. Average of BRDD-DBNDSTO method under 70%TRAPH and 30%TESPH

The training $accu_y$ (TRAAC) and validation $accu_y$ (VLAAC) performance of the BRDD-DBNDSTO model is depicted in Fig. 5. The $accu_y$values are figured through the interval of 0-25 epoch counts. The figure highlighted the TRAAC and VLAAC values show growing tendencies that indicate the capabilities of the BRDD-DBNDSTO algorithm with enhanced performance across various iterations. Moreover, the TRAAC and VLAAC stay adjacent across the epoch counts, which indicates lesser overfitting and demonstrates maximum performance of the BRDD-DBNDSTO algorithm, assuring consistent prediction on undetected instances.

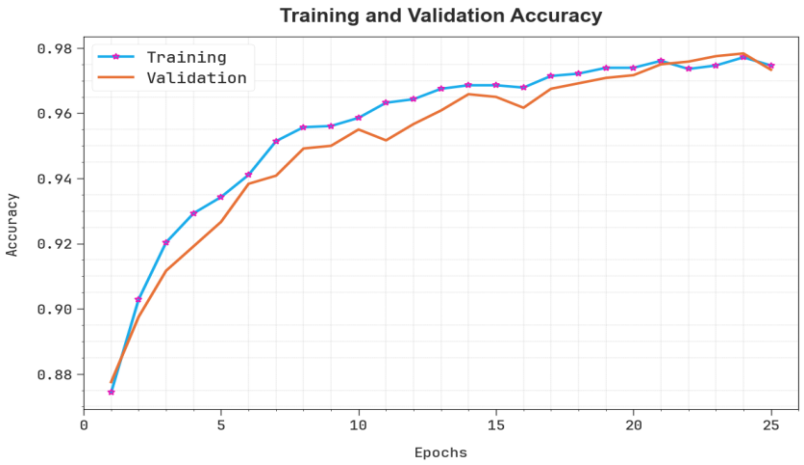

Figure 5. $Accu_y$ Curve of BRDD-DBNDSTO method

DOI: https://doi.org/10.54216/IJNS.250318
Received: June 06, 2024 Revised: August 27, 2024 Accepted: October 04, 2024

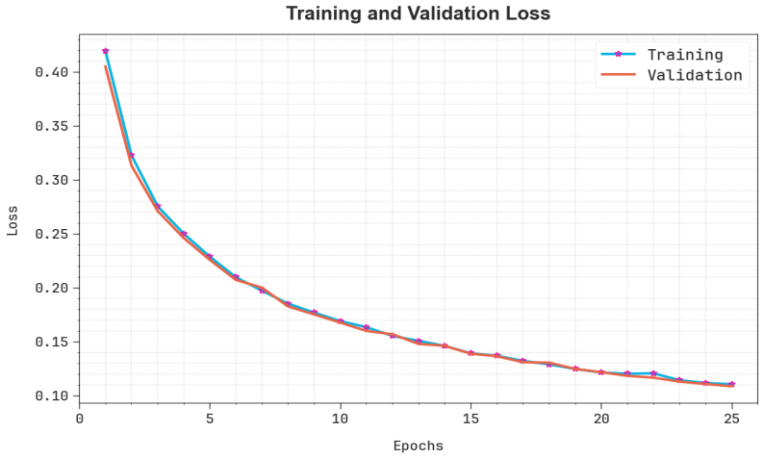

Figure 6. Loss curve of BRDD-DBNDSTO method

In Fig. 6, the TRA loss (TRALS) and VLA loss (VLALS) graphs of the BRDD-DBNDSTO technique are shown. The loss values are calculated for 0-25 epochs. It is showcased that the TRALS and VLALS values establish subsiding tendencies, disclosing the proficiency of the BRDD-DBNDSTO method in balancing a trade-off between data fitting and generality. The repeated fall in loss values pledges the advanced functioning of the BRDD-DBNDSTO model and tuning the prediction results gradually.

Table 3 and Fig. 7 examine the comparison results of the BRDD-DBNDSTO method using recent models [21]. The study featured that the RetinaNet, MobileNet, AlexNet, GoogleNet, and RDD-HGSENN methods have stated worse performance. Although, OFWNN-RDD algorithm has got closer results. Additionally, the BRDD-DBNDSTO technique stated superior performance with greatest $accu_y$, $prec_n$, $reca_l$, and $F1_{score}$ of 98.92%, 97.85%, 97.82%, and 97.83% correspondingly.

Table 3: Comparative analysis of BRDD-DBNDSTO model with recent models

Methods	$Accu_y$	$Prec_n$	$Reca_l$	$F1_{score}$
BRDD-DBNDSTO	98.92	97.85	97.82	97.83
OFWNN-RDD	98.64	97.23	97.22	97.20
RDD-HGSENN	98.09	96.32	96.41	96.36
AlexNet Model	92.91	93.59	93.91	93.01
GoogleNet Method	91.53	92.31	91.39	91.47
RetinaNet Algorithm	90.76	89.52	89.85	90.23
MobileNet Classifier	90.09	90.93	89.03	89.21

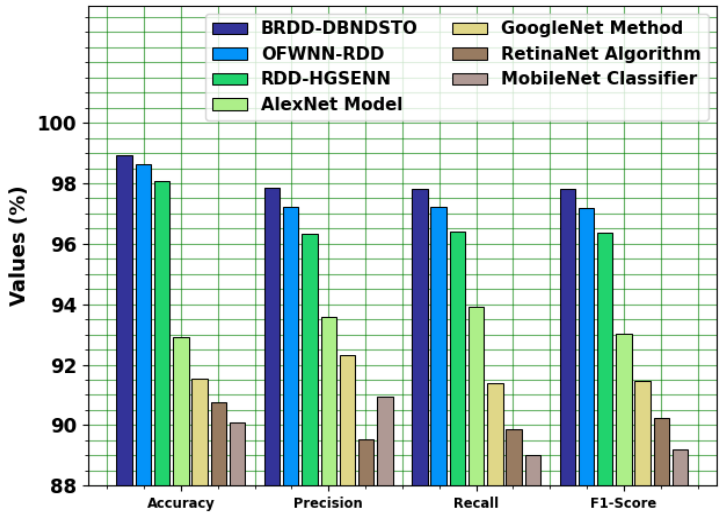

Figure 7. Comparative analysis of BRDD-DBNDSTO model with recent methods

DOI: https://doi.org/10.54216/IJNS.250318
Received: June 06, 2024 Revised: August 27, 2024 Accepted: October 04, 2024

5. Conclusion

In this article, we have introduced a new BRDD-DBNDSTO algorithm. The proposed BRDD-DBNDSTO method is mainly intended to enhance the accuracy and reliability of road damage classification for intelligent smart city infrastructure. To accomplish this, the BRDD-DBNDSTO technique employs ABF using image preprocessing to effectively enhance image quality by reducing noise. Then, the SqueezeNet method was used to create a collection of feature vectors. For the classification and detection of road damage, the DEMATEL with BND model is exploited. Eventually, the STO model can be used to adjust the parameters associated with the classifier method. To guarantee the improved performance of the BRDD-DBNDSTO method, an extensive experimental study was carried out and the gained outcomes illustrate the improvement of the BRDD-DBNDSTO model across the existing techniques.

Funding: "This research received no external funding"

Conflicts of Interest: "The authors declare no conflict of interest."

References

[1] Chinnadurai, V. and Sindhu, M.P., 2020. An introduction to neutro-fine topology with separation axioms and decision making. International Journal of Neutrosophic Science (IJNS) Volume 12, 2020, p.11.

[2] K. Atanassov, P. Krawczak, and S. Sotirov, "Intuitionistic fuzzy sets and their generalizations in decision making and soft computing," Fuzzy Sets and Systems, vol. 410, pp. 1–22, 2022, doi: 10.1016/j.fss.2021.11.007.

[3] Edalatpanah, S.A., 2020. A direct model for triangular neutrosophic linear programming. International journal of neutrosophic science, 1(1), pp.19-28.

[4] Dhanalakshmi, G., Sandhiya, S. and Smarandache, F., 2024. Selection of the best process for desalination under a Treesoft set environment using the multi-criteria decision-making method. International Journal of Neutrosophic Science, 23(3), pp.140-40.

[5] Almuhur, E., Miqdad, H., Al-labadi, M. and Idrisi, M.I., 2024. μ-L-Closed Subsets of Noetherian Generalized Topological Spaces. International Journal of Neutrosophic Science, 23(3), pp.148-48.

[6] B. Abu-Salih, P. Wongthongtham, K. Coutinho, R. Qaddoura, O. Alshaweesh, and M. Wedyan, ''The development of a road network flood risk detection model using optimised ensemble learning,'' Eng. Appl. Artif. Intell., vol. 122, Jun. 2023, Art. no. 106081.

[7] M. Al Duhayyim, A. A. Malibari, A. Alharbi, K. Afef, A. Yafoz, R. Alsini, O. Alghushairy, and H. Mohsen, ''Road damage detection using the hunger games search with Elman neural network on high-resolution remote sensing images,'' Remote Sens., vol. 14, no. 24, p. 6222, Dec. 2022.

[8] K. Zhao, J. Liu, Q. Wang, X. Wu, and J. Tu, ''Road damage detection from post-disaster high-resolution remote sensing images based on TLD framework,'' IEEE Access, vol. 10, pp. 43552–43561, 2022.

[9] G. Ochoa-Ruiz, A. A. Angulo-Murillo, A. Ochoa-Zezzatti, L. M. Aguilar-Lobo, J. A. Vega-Fernández, and S. Natraj, ''An asphalt damage dataset and detection system based on RetinaNet for road conditions assessment,'' Appl. Sci., vol. 10, no. 11, p. 3974, Jun. 2020.

[10] K. Hacıefendioğlu and H. B. Başağa, ''Concrete road crack detection using deep learning-based faster R-CNN method,'' Iranian J. Sci. Technol., Trans. Civil Eng., vol. 46, no. 2, pp. 1621–1633, Apr. 2022.

[11] Merolla, D., Latorre, V., Salis, A. and Boanelli, G., 2024. Automated Road Safety: Enhancing Sign and Surface Damage Detection with AI. arXiv preprint arXiv:2407.15406.

[12] Chu, H.H., Saeed, M.R., Rashid, J., Mehmood, M.T., Ahmad, I., Iqbal, R.S. and Ali, G., 2023. Deep learning method to detect the road cracks and potholes for smart cities. Comput Mater Contin, 75(1), pp.1863-1881.

[13] Adewopo, V.A. and Elsayed, N., 2024. Smart city transportation: Deep learning ensemble approach for traffic accident detection. IEEE Access.

[14] Silva, L.A., Leithardt, V.R.Q., Batista, V.F.L., González, G.V. and Santana, J.F.D.P., 2023. Automated road damage detection using UAV images and deep learning techniques. IEEE Access, 11, pp.62918-62931.

[15] Jagatheesaperumal, S.K., Bibri, S.E., Huang, J., Rajapandian, J. and Parthiban, B., 2024. Artificial intelligence of things for smart cities: advanced solutions for enhancing transportation safety. Computational Urban Science, 4(1), p.10.

[16] Chen, C., Yao, G., Liu, L., Pei, Q., Song, H. and Dustdar, S., 2023. A cooperative vehicle-infrastructure system for road hazards detection with edge intelligence. IEEE Transactions on Intelligent Transportation Systems, 24(5), pp.5186-5198.

DOI: https://doi.org/10.54216/IJNS.250318
Received: June 06, 2024 Revised: August 27, 2024 Accepted: October 04, 2024

[17] Gollamandala, U.B., Midasala, V. and Ratna, V.R., 2022. FPGA implementation of hybrid recursive reversable box filter-based fast adaptive bilateral filter for image denoising. Microprocessors and Microsystems, 90, p.104520.

[18] Chahil, S.T.H., Zakwan, M., Khan, K. and Fazil, A., 2024. Performance analysis of different signal representations and optimizers for CNN based automatic modulation classification.

[19] Yaacob, S.N., Hashim, H., Sulaiman, N.H., Awang, N.A., Al-Quran, A. and Abdullah, L., 2025. An Integrated DEMATEL with Bipolar neutrsophic Dombi-based Heronian Mean Operator and Its Applications in Decision-making Problem. International Journal of Neutrosophic Science, (1), pp.08-8.

[20] Lv, Y., Shen, Y., Zhang, A., Ren, L., Xie, J., Zhang, Z., Zhang, Z., An, L., Sun, J., Yan, Z. and Mi, O., 2024. Rock dynamic strength prediction in cold regions using optimized hybrid algorithmic models. Geomechanics and Geophysics for Geo-Energy and Geo-Resources, 10(1), pp.1-29.

[21] Alamgeer, M., Alkahtani, H.K., Maashi, M., Othman, M., Hilal, A.M., Alsaid, M.I., Osman, A.E. and Alneil, A.A., 2023. Optimal fuzzy wavelet neural network based road damage detection. IEEE Access, 11, pp.61986-61994.

DOI: https://doi.org/10.54216/IJNS.250318
Received: June 06, 2024 Revised: August 27, 2024 Accepted: October 04, 2024